Draft version December 10, 2008
Preprint typeset using LaTeX style emulateapj v. 10/10/03

THEORETICAL MODELING OF PROPAGATION OF MAGNETO-ACOUSTIC WAVES IN MAGNETIC REGIONS BELOW SUNSPOTS.

E. Khomenko[1,2], A. Kosovichev[3], M. Collados[1], K. Parchevsky[3] and V. Olshevsky[2]

Draft version December 10, 2008

ABSTRACT

We use 2D numerical simulations and eikonal approximation, to study properties of MHD waves traveling below the solar surface through the magnetic structure of sunspots. We consider a series of magnetostatic models of sunspots of different magnetic field strengths, from 10 Mm below the photosphere to the low chromosphere. The purpose of these studies is to quantify the effect of the magnetic field on local helioseismology measurements by modeling waves excited by sub-photospheric sources. Time-distance propagation diagrams and wave travel times are calculated for models of various field strength and compared to the non-magnetic case. The results clearly indicate that the observed time-distance helioseismology signals in sunspot regions correspond to fast MHD waves. The slow MHD waves form a distinctly different pattern in the time-distance diagram, which has not been detected in observations. The numerical results are in good agreement with the solution in the short-wavelength (eikonal) approximation, providing its validation. The frequency dependence of the travel times is in a good qualitative agreement with observations.

Subject headings: MHD; Sun: magnetic fields; Sun: oscillations; Sun: helioseismology

1. INTRODUCTION

Local helioseismology (time-distance helioseismology, acoustic holography and ring-diagram analysis) provides valuable information about the physical properties of solar sub-surface layers (*e.g.* Duvall et al. 1993; Kosovichev 1999, 2002; Kosovichev et al. 2000; Zhao & Kosovichev 2003; Braun & Lindsey 2000; Hill 1988; Haber et al. 2000). Time-distance helioseismology (Duvall et al. 1993; Kosovichev & Duvall 1997) makes use of wave travel times measured for wave packets traveling between various points on the solar surface through the interior. By inversion of these measurements, variations of the wave speed and velocities of mass flows can be recovered below the visible solar surface. Inversion results for the travel times have been obtained for quiet Sun regions as well as for magnetic active regions including sunspots. In most of these cases, the variations of the travel times were assumed to be caused by mass flows and magneto-sonic speed fluctuations along the wave paths. It is known that sunspots possess strong magnetic fields with a complicated structure in the visible layers of the Sun where the Doppler measurements used by local helioseismology are taken (Solanki 2003). Consequently, such magnetic field can cause important effects on helioseismic waves, beyond the perturbation theories employed for helioseismic data analysis (Kosovichev & Duvall 1997; Birch & Kosovichev 2000; Gizon & Birch 2002). Magnetic field can change the acoustic excitation rate and spectral properties of solar oscillations (see the recent work by Jacoutot et al. 2008); produce new wave modes; change wave propagation speeds; change the wave propagation paths and reflection characteristics at the near-surface layers.

Electronic address: khomenko@iac.es
[1] Instituto de Astrofísica de Canarias, 38205, C/ Vía Láctea, s/n, Tenerife, Spain
[2] Main Astronomical Observatory, NAS, 03680, Kyiv, Ukraine
[3] Stanford University, 455 Via Palou, Stanford, CA 94305, United States

The influence of magnetic field on the interpretation of local helioseismology measurements has not been fully explored. Theoretical efforts have been made by Crouch & Cally (2003), Cally (2005, 2006), Schunker & Cally (2006), Cally & Goossens (2008), Schunker et al. (2008) to include mode conversion and model waves in magnetized structures by means of analytical and ray-path theories. These studies confirm the potential importance of magnetic effects. A more complete understanding of the problem can be reached by direct forward modeling of helioseismic data, by solving numerically the MHD equations in realistic magnetic configurations (*e.g.*, Gizon et al. 2006; Khomenko & Collados 2006; Hanasoge 2008; Cameron et al. 2007; Parchevsky & Kosovichev 2008). In these papers, the MHD equations, governing the problem, are solved for magnetic field configurations resembling a sunspot or a part of a sunspot. The results have demonstrated how magnetic fields change the speed, amplitude and spectral properties of the waves, and also produce wave transformation and refraction in the sunspot atmosphere.

Observational helioseismology over active regions has demonstrated repeatedly that waves travel faster through sunspots in comparison with quiet Sun measurements (*e.g.* Duvall et al. 1993; Braun 1997). This fact is still the subject of present investigations and its explanation is still far from clear. Although, given that sunspots possess an intense field at photospheric levels, direct or indirect the influence of the magnetic field is generally accepted (*e.g.* Hindman et al. 1997). At sub-photospheric levels the influence of the magnetic field becomes less and less important with depth as pressure forces dominate over magnetic forces. This is why the phenomena related to magnetic field are referred to as "surface effects". Explanations based on wave perturbations due to scattering phase shifts (Braun 1997; Lindsey & Braun 2005a,b) taking place within a few Mm below the photosphere or local wave speed variations below sunspots

(Kosovichev et al. 2000) have been suggested to explain the different travel times measured in sunspots and in the quiet photosphere.

In this paper, we study wave properties and variations of travel times with the help of numerical simulations and Eikonal solutions for wave propagation in sunspot-like magnetic structures in stratified surface and subsurface layers. We perform 2D numerical simulations of the waves produced by a single source for a series of model sunspots (Khomenko & Collados 2008). We study various types of MHD waves and their propagation properties numerically. In addition, for the fast magneto-acoustic mode we obtain a solution in the eikonal approximation, which is often important for correct interpretation of helioseismic results (Gough 2007). Our numerical results clearly indicate that the fast mode is the primary source of helioseismic signals. We study the frequency dependence of the wave travel times and compare the results of the eikonal approach with our numerical simulations and observational data. Our results provide insight into the properties of helioseismic waves in magnetic regions and are important for interpretation of time-distance helioseismology measurements.

2. NUMERICAL PROCEDURE

We use the numerical simulation code described previously by Khomenko & Collados (2006); Khomenko et al. (2008). The code solves the basic non-linear equations of the ideal MHD, written in conservative form:

$$\frac{\partial \rho}{\partial t} + \vec{\nabla}\cdot(\rho\vec{V}) = 0\,, \tag{1}$$

$$\frac{\partial(\rho\vec{V})}{\partial t} + \vec{\nabla}\cdot[\rho\vec{V}\vec{V} + (P+\frac{\vec{B}^2}{8\pi})\mathbf{I} - \frac{\vec{B}\vec{B}}{4\pi}] = \rho\vec{g}\,, \tag{2}$$

$$\frac{\partial E}{\partial t} + \vec{\nabla}\cdot[(E+P+\frac{\vec{B}^2}{8\pi})\vec{V} - \vec{B}(\frac{\vec{B}\cdot\vec{V}}{4\pi})] = \rho\vec{V}\cdot\vec{g} + \rho Q\,, \tag{3}$$

$$\frac{\partial \vec{B}}{\partial t} = \vec{\nabla}\times(\vec{V}\times\vec{B})\,, \tag{4}$$

where $\mathbf{I}$ is the identity tensor and E is the total energy:

$$E = \frac{1}{2}\rho V^2 + \frac{P}{\gamma-1} + \frac{B^2}{8\pi}\,. \tag{5}$$

All other symbols have their usual meaning. Gravity has been taken constant, with a value of 2.74×10^4 cm/sec^2. The term describing radiative energy losses, Q, is set to zero in the present study. A Perfectly Matching Layer (PML) boundary condition (Berenger 1994) is applied to all boundaries of the simulation domain with the aim of minimizing wave reflection effects at the boundaries. This performs rather well in our simulations. The thickness of the PML layer in our simulations is 20 grid points (1 Mm).

The code solves the non-linear MHD equations for perturbations, that are obtained by subtracting the equations of initial magnetostatic equilibrium from Eqs. 1-4. However, for the purpose of the present study, we keep the perturbation amplitudes as low as possible, making the 2nd order non-linear terms relatively unimportant. In this paper, we use the 2D version of the code.

The wave source is modeled as a time-dependent term $\vec{S}(x,z,t)$ in the right hand side of the momentum equation (Eq. 2) in the same way as in the paper by Parchevsky & Kosovichev (2008):

$$f(x,z,\tau) = \begin{cases} A\left[1-\dfrac{r^2}{R_{src}^2}\right]^2\left(1-2\tau^2\right)e^{-\tau^2} & \text{if } r \le R_{src} \\ 0 & \text{if } r > R_{src}, \end{cases} \tag{6}$$

where R_{src} is the source radius, taken to be 250 km; r is the distance from the source center, $r = \sqrt{(x-x_{src})^2+(z-z_{src})^2}$. The parameter τ is given by the equation

$$\tau = \frac{\omega(t-t_0)}{2} - \pi, \qquad t_0 \le t \le t_0 + \frac{4\pi}{\omega}, \tag{7}$$

where ω is the central, dominating, frequency of the source and t_0 is the source start moment. In our model the source represents the vertical force in the momentum equation, $\vec{S} = (0, f)^T$. The central frequency of the source is 3.3 mHz. In all the simulations described here, the center of the source is located at depth -200 km, below the photospheric level of the reference model S of Christensen-Dalsgaard et al. (1996). The depth location of the source in our simulations corresponds to the recent studies of the excitation of waves in magnetic regions by Jacoutot et al. (2008).

The source generates a broad spectrum of acoustic and surface gravity waves in the 5-minute range, resembling the wave excitation in the real Sun. In the case of a sunspot model, these modes are modified by the presence of magnetic field.

3. SUNSPOT MODEL AND SIMULATION SETUP

The sunspot models are calculated using the method proposed in Khomenko & Collados (2008). Here we use three magnetostatic models of sunspots with similar magnetic field structure but different values of the magnetic field strength. In this way we are able to study the effects of the magnetic field strength on the propagating waves apart from the effects of the magnetic field inclination. Some characteristics of these models are displayed in Figures 1 and 2. The magneto-static equilibrium is calculated in the cylindrical coordinates assuming azimuthal asymmetry and no twist of the magnetic field lines. At large distances from the axis, the sunspot models merge smoothly into the quiet Sun model, for which we take the model S of Christensen-Dalsgaard et al. (1996), modified to make it stable with respect to convective motions (see Parchevsky & Kosovichev 2007). The sound speed variations along the radial distance are evident from Fig. 2. The sunspot models have a low-temperature zone below the surface down to, about, -2 Mm depth. Below this depth the temperature gradient in the horizontal direction is small and no high-temperature zone is introduced in the present study. Note that the ratio between the acoustic and the Alfvén speeds squared changes by orders of magnitude with height, and that the gradient of this ratio is largest in the surface layers.

For the wave simulations, the models are transformed from cylindrical coordinates (r,ϕ,z) to 3D cartesian coordinates. In a general case, all three components of the magnetic field vector are non-zero in the cartesian coordinates. In the case of the 2D simulations, we chose a slice where the B_y component of the field is equal to zero and calculate the wave propagation in this plane.

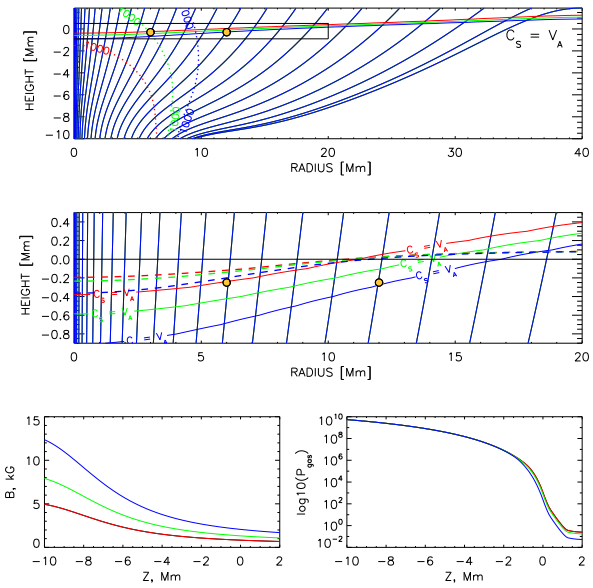

FIG. 1.— Top panel: topology of the magnetic field lines for the three sunspot models with $B_{\rm phot}$=0.9 kG (red lines), 1.5 kG (green lines) and 2.4 kG (blue lines). The horizontal solid lines mark the levels where $c_S = v_A$. The contours of the magnetic field strength of $B = 1$ kG are shown by dotted curves for each case. Two yellow dots mark the locations of the wave source in the two sets of our simulations. Middle panel: enlarged view of the upper part of the sunspot models marked by the box in the top panel. The vertical axis has been expanded for better visualization. Dashed lines are the contours of constant optical depth $\log\tau_5 = -1.6$. Bottom panels: the height dependence of the magnetic field strength and the gas pressure at the axis for these models.

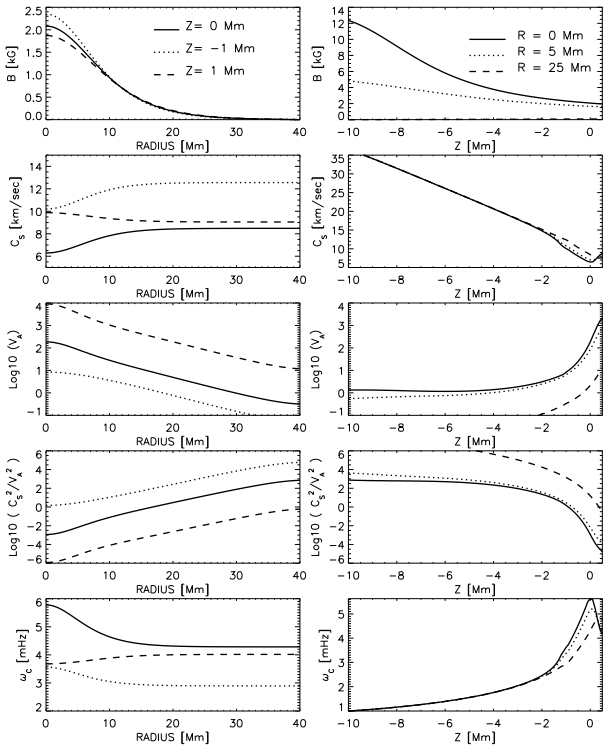

FIG. 2.— The distribution with the radial distance (left panels) and with the depth (right panels) of the magnetic field strength, B; sound speed, c_S; Alfvén speed, v_A; their ratio, c_S^2/v_A^2; and the acoustic cut-off frequency, ω_c (calculated in the assumption of an isothermal atmosphere) for the $B_{\rm phot}$=2.4 kG sunspot.

By adopting this approach we exclude Alfvén waves from consideration.

The simulation domain is 40 Mm in the horizontal direction and 10.5 Mm in the vertical direction. The sunspot axis is located at the center of the simulation domain, and the upper 0.5 Mm of the domain are located above $Z = 0$ km height. Above $Z = 0.5$ Mm we introduce an isothermal PML layer, 1 Mm thick. The grid resolution of the simulations is 50 km in the vertical and 100 km in the horizontal directions. The temporal resolution depends on the CFL numerical stability condition, limited by the rapid growth of the Alfvén speed, v_A, with height, changing typically between 0.01 and 0.08 seconds. For each of the three sunspot models we perform two simulation runs with the wave source located at $X_0 = 6$ Mm and 12 Mm to the left of the sunspot axis.

In addition to the simulations of waves in the sunspot models, we have also performed a reference simulation for a model without magnetic field and without horizontal variations in thermodynamic parameters. The vertical stratification of the thermodynamic parameters in this case corresponds to the modified model S.

Several recent works on helioseismology point out the presence of the so-called "surface effects" in the measurements in active regions (see *e.g.* Lindsey & Braun 2005a,b; Schunker et al. 2005; Zhao & Kosovichev 2006; Rajaguru et al. 2007). Due to the Wilson depression in sunspots the formation heights of spectral lines are altered introducing additional phase shifts into the velocity measurements, as compared to non-magnetic regions. Our sunspot models describe the Wilson depression effect since the whole atmosphere inside the magnetic concentration had been shifted downwards. In order to take these "surface effects" into account, we have computed the optical depth scale τ_5 in our sunspot models. This has been done with the help of SIR code (Ruiz Cobo & del Toro Iniesta 1992). As expected, the τ_5 scale varies with radial distance from sunspot center. This variation can be appreciated at the middle panel of Fig. 1, where the contours of the constant optical depth $\log\tau_5 = -1.6$ are given. The optical depth $\log\tau_5 = -1.6$ represents the layer where typical photospheric spectral lines are formed. In the rest of the paper we call "photospheric velocity" the velocity measured at $\log\tau_5 = -1.6$ level. Note that the height variations in the position of this layer can be as large as 0.2–0.4 Mm, depending on the distance from the axis in the sunspot models. In the non-magnetic simulation the "photospheric velocity" at $\log\tau_5 = -1.6$ always corresponds to the same height, as there is no Wilson depression.

4. WAVE FIELD FROM A SINGLE SOURCE

In this section we describe the results of the simulations for the three model sunspots and the quiet Sun model for two positions of the oscillation source. In the first series of simulations, the source is located in the "umbral" part of the model at a distance of 6 Mm from the sunspot axis, where the field is relatively strong. In this region the ratio c_S^2/v_A^2 is equal to 1.4, 0.46 and 0.11 in the three models with $B_{\rm phot} = 0.9$, 1.5 and 2.4 kG, correspondingly. Thus, the wave source is located in the region dominated by the magnetic field in the last two models. In the second series, the source is located in the "penumbral" part of the model, at a distance of 12 Mm

from the axis, where the field is weaker. There the parameter c_S^2/v_A^2 is equal to 8.2, 3.1 and 1.1 in the three models. In this case the waves are excited in the acoustically dominated region. Placing the wave source at these two positions allows us to study the wave properties for the two different regimes. Note, that through the whole paper we choose to discuss the results in terms of the parameter c_S^2/v_A^2 instead of plasma β. The former parameter is more relevant regarding wave propagation. The ratio between these two parameters is equal to $(c_S^2/v_A^2)/\beta = \gamma/2 = 5/6$ (for an ideal gas). The layers $c_S^2/v_A^2 = 1$ and $\beta = 1$ are located very close in the atmosphere. The maximum height separation between them is about 30 km. The locations of the sources in both sets of simulations are marked by yellow dots in Fig. 1. The duration of each simulation run is about 50 minutes.

4.1. *Non-magnetic case*

Fig. 3 shows the time evolution of the simulated horizontal and vertical velocities in the case of the quiet Sun model. In the figure, the velocities are scaled with the square root of the background density in order to make visible variations in the deep layers. The simulation reveals that the single acoustic source excites a mixture of acoustic (p), gravity (g) and surface (f) modes, each propagating with its own speed. The p modes are the fastest and run beyond the boundaries of the simulation domain after about 30 min. The slower g and f modes are concentrated in the upper part of the simulation domain. It can be seen that the wave field is symmetric with respect to the source location since the medium is isotropic for the acoustic-gravity waves.

The power spectrum of the photospheric vertical velocity ($k-\nu$ diagram) in the non-magnetic simulations is given in Fig. 4. The diagram demonstrates the presence of several ridges of acoustic (p-mode) oscillations. The darkest bottom ridge corresponds to f mode. The f-mode analytical dispersion relation is also plotted in the image and shows a reasonable agreement with the numerical results. The figure also reveals the presence of a weak g-mode signal below the f-mode ridge. These modes appear because the background model has been made convectively stable.

4.2. *Waves in sunspot models*

Figures 5 and 6 show the results of the simulations in the sunspot model with $B_{\rm phot} = 1.5$ kG and the source location at $X_0 = 6$ Mm and 12 Mm, correspondingly. In the case of the simulations with magnetic field, we use for illustrations the longitudinal (parallel to the local field) and transversal (perpendicular to the field) velocity components. This provides an effective separation of the fast and slow magneto-acoustic waves in those regions of the simulation domain where the characteristic propagation speeds are clearly distinct ($v_A \ll c_S$ or $v_A \gg c_S$). Apart from a smaller propagation speed, the slow mode is mainly magnetic in the region where $v_A \ll c_S$, and has a displacement velocity that is perpendicular to the magnetic field lines. This means that it contributes mainly to the transversal velocity. On the other hand, the fast mode is mainly acoustic, i.e., longitudinal, by its nature. As this can be seen in Fig. 5, the longitudinal component of the fast mode vanishes approximately along the field line crossing the source. The direction of propagation of the slow magneto-acoustic waves (defined as the direction of their group velocity) is always parallel to the magnetic field direction, irrespective of their phase velocity. The direction of propagation of the fast magneto-acoustic waves is independent of the field direction, and the group velocity is parallel to the phase velocity. Given these properties, the fast and slow modes can be distinguished in the time evolution pictures of the transversal and longitudinal velocity components, displayed in Figures 5 and 6.

In all simulations, the wave source is located in the region where c_S^2/v_A^2 stay (roughly) between 0.1 and 10, and the field is significantly inclined. In this region, both the pressure and magnetic restoring forces are of the same order of magnitude. Thus, the source generates a set of fast and slow magneto-acoustic waves. The fast modes are an analog of the acoustic p-modes in the non-magnetic simulations (see Fig. 3). However, as it will be shown later in the paper, their behavior is modified by the presence of the magnetic field. The slow modes did not appear in the non-magnetic simulation.

Fig. 5 shows that the fast wave propagating in this complex magnetic field configuration causes variations in both, longitudinal and transversal, components of the velocity of the same order of magnitude. The initial wave front expands propagating downwards. There is no symmetry in the wave field with respect to the source location (unlike the case of the non-magnetic simulation) since the wave propagation speed now depends on the direction. In the deep layers, the dominant velocity variations are due to the fast mode waves. In the upper photospheric layers we observe mostly variations in the longitudinal velocity (right panels in Fig. 5). The transversal velocity variations, caused by the fast magnetic waves ($c_S^2/v_A^2 \ll 1$), are negligible in these layers. The wave velocity field developed in the simulations with the source located at $X_0 = 6$ and 12 Mm from the sunspot axis are similar. The differences are quantitative, not qualitative in nature.

Fig. 6 gives a more detailed view on the evolution of the transversal velocity component in the upper part of the simulation domain (note that the vertical axis has been expanded) and allows to understand better the complex physics of the wave propagation in the vicinity of the $c_S = v_A$ layer. An even better view on the wave dynamics in this region can be gained by watching the movie of the simulation, provided as on-line material to this paper. We observe in Fig. 6 the presence of the slow MHD mode generated directly by the source. This mode propagates with a visibly low speed downwards along the sunspot magnetic field lines. It is localized close to the horizontal position $X = -10$ Mm.

The fast waves generated by the source experience a significant refraction and reflection due to the strong increase of the Alfvén speed (see Fig. 2) in the vicinity of the $c_S = v_A$ layer (snapshots corresponding to times between 8 and 14 minutes in Fig. 6).

In addition to the slow MHD waves generated directly by the source there is another wave type. It can be observed in Fig. 5 between 14 and 24 minutes of time as a perturbation with much smaller vertical wavelength compared to that of the fast modes in the sunspot interior. We can observe from Fig. 5 that the propagation speed of

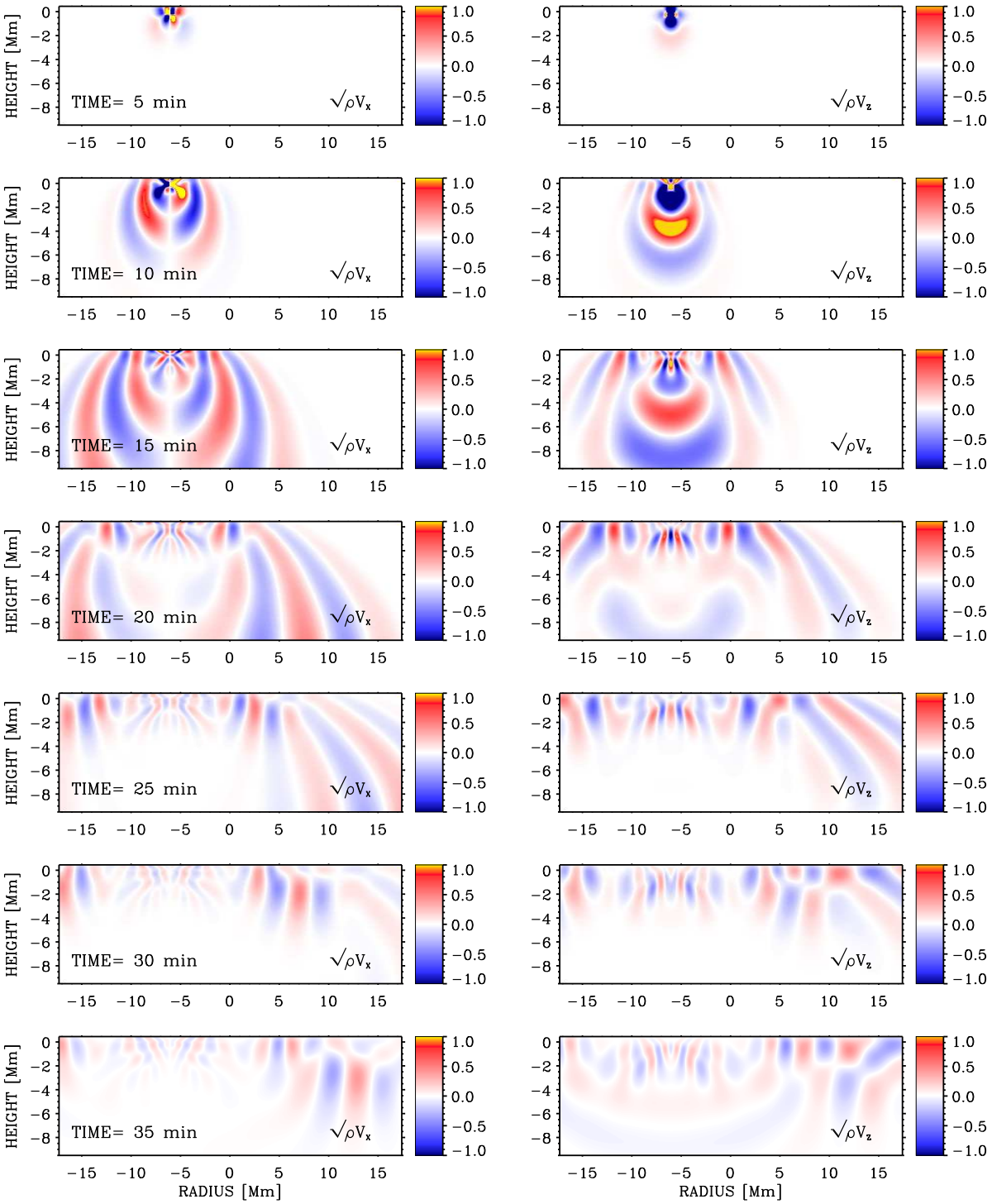

FIG. 3.— Time series of snapshots of the horizontal (left panels) and vertical (right panels) velocities in the non-magnetic simulations with $X_0 = 6$ Mm. The velocities are scaled with $\sqrt{\rho_0}$, the color scale is the same in both panels. The negative heights correspond to sub-photospheric layers.

this low-wavelength disturbance is comparable to that of the fast modes. Unlike the slow MHD waves, these waves propagate horizontally across the sunspot. Thus, these waves are different from either fast or slow MHD waves in several aspects: (1) they have a vertical wavelength that is much smaller than that of the fast waves; (2) they propagate with speeds similar to the fast waves (note, however, that they propagate in the region where the sound speed is slightly larger than the Alfvén speed); (3) they propagate across the field, a behavior impossible for slow waves in this region; (4) the waves that posses similar characteristics (superficial horizontal propagation, smaller wavelength, etc) in non-magnetic simulations are the f-mode waves. From these arguments we suggest that we see a wave type with properties that are a mixture of magnetic and f-mode waves. We call them "sur-

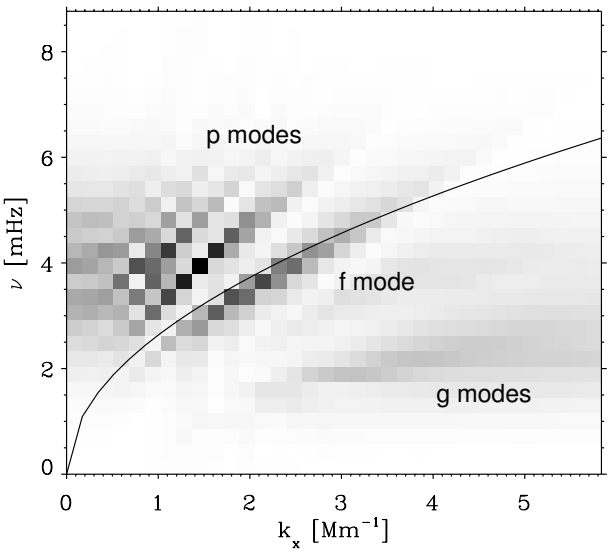

FIG. 4.— The $k-\nu$ power spectrum of the photospheric vertical velocity in the non-magnetic standard solar model simulation run. Darker colors indicate larger power. The black line indicates the dispersion relation of the f-mode: $\omega^2 = gk_x$, where g is the value of solar gravity acceleration at the surface. Several p modes can be distinguished above the f mode. The g modes, located below the f mode are also excited by the vertical force source. These modes are present because the solar model has been made convectively stable.

face magneto-gravity" waves. These waves were mentioned previously by, *e.g.* Schwartz & Stein (1975), who described their properties in an isothermal atmosphere. The variations produced by the surface magneto-gravity waves decrease rapidly with depth and disappear almost completely below −3 Mm.

The power spectra of the photospheric vertical velocity in the magnetic simulations for different $B_{\rm phot}$ and the source location at 12 Mm from the sunspot axis are compared in Fig. 7. Figure 7 shows that for the magnetic models the $k-\nu$ diagrams become progressively more and more different from the non-magnetic $k-\nu$ diagram (Fig. 4), with increasing magnetic field strength. Even in the case of the weakest field, $B_{\rm phot} = 0.9$ kG, the inclination of the p-mode ridges is larger than in the pure acoustic case. The inclination of the ridges increases with increasing magnetic field strength. The dispersion relation for the p-mode ridges depends on the reflection conditions for waves in the upper layers. In the absence of magnetic field, the waves with different frequencies reflect at different heights in the photosphere and below due to the rapid change of the cut-off frequency with height. When the magnetic field is introduced, the upper reflection condition changes even if the field is as weak as in the $B_{\rm phot} = 0.9$ kG model. This happens because the propagation path of the high frequency fast waves is modified strongly by the rapid increase of the Alfvén speed since these waves penetrate higher up in the atmosphere. The reflection height for such waves becomes lower compared to the non-magnetic case. This naturally produces the change of the dispersion relation observed at the $k-\nu$ diagrams in Fig. 7.

4.3. *Time-distance diagrams and travel time estimates*

In order to quantify the effects of magnetic field on the travel time measurements of local helioseismology, we have constructed time-distance diagrams for the vertical velocity. Such diagrams were constructed for the photospheric velocity measured at the optical depth $\log\tau_5 = -1.6$ (see Sect. 3) in the sunspot models. Since in our simulations the waves are excited by a single source, there is no need to compute the velocity correlations between the different surface points. Thus, the time-distance wave propagation diagrams are constructed by plotting the velocity variations as a function of time for all horizontal points at constant $\log\tau_5$ level. Fig. 8 shows the time-distance diagrams in the non-magnetic simulations and the simulations with progressively increasing magnetic field strength.

In the time-distance diagram for the non-magnetic case (Fig. 8, a), the two lowest system of ridges are due to the p modes. The green dashed line in Fig. 8a gives a theoretical dispersion relation for these modes, calculated for the standard solar model S. Above them, the third system of ridges comes from the f mode waves. It can be seen from the inclination of the ridges that the phase and group speeds of this mode are different from those of the p modes, confirming that they belong to the f-mode. The theoretical time-distance curve for the f-mode (blue dashed line in Fig. 8a) is in a good agreement with the numerical results. The system of ridges at the top part of the diagram above the source corresponds to the g modes. These modes propagate with much lower speed than the p and f modes, in agreement with their appearance at the $k-\nu$ diagram in Fig. 4.

The time-distance diagrams in the simulations with magnetic field have different properties (Fig. 8, b, c, and d). p-mode-like ridges are present in all the cases. As in the non-magnetic case, we have added theoretical curves for p-modes and the f-mode in the absence of the magnetic field (green and blue dashed curves, in Fig. 8b, c, and d). These curves help identifying the fast modes as the analog of the non-magnetic p-modes propagating with a speed modified by the magnetic field. The f- and g-mode ridges do not appear, in agreement with the $k-\nu$ diagram in Fig. 7. Instead, weak traces of the slow waves are present in the top part of the diagram. This mode is not symmetric with respect to the source location and has only surface signatures on the side of the source where the magnetic field is larger. At the $\log\tau_5 = -1.6$, the slow mode is mostly prominent in the sunspot simulation with weak field $B_{\rm phot} = 0.9$ kG. It becomes weaker but still can be distinguished in the models with stronger field. The origin of this mode is different from the slow modes generated by the source in the sunspot interior (Fig. 6) and needs further study.

At first glance, the p-mode ridges on the time-distance diagrams seem not to be affected much by the magnetic field. A more detailed investigation shows that the p-mode ridge, at the bottom, becomes thicker, *i.e.* the relative contribution of the different frequencies in the wave packet changes with magnetic field. We have performed a fit to the time-distance diagrams in order to find the phase and group travel times of waves in each case. At each horizontal position starting from 3 Mm from the source we fit the time velocity curve with a

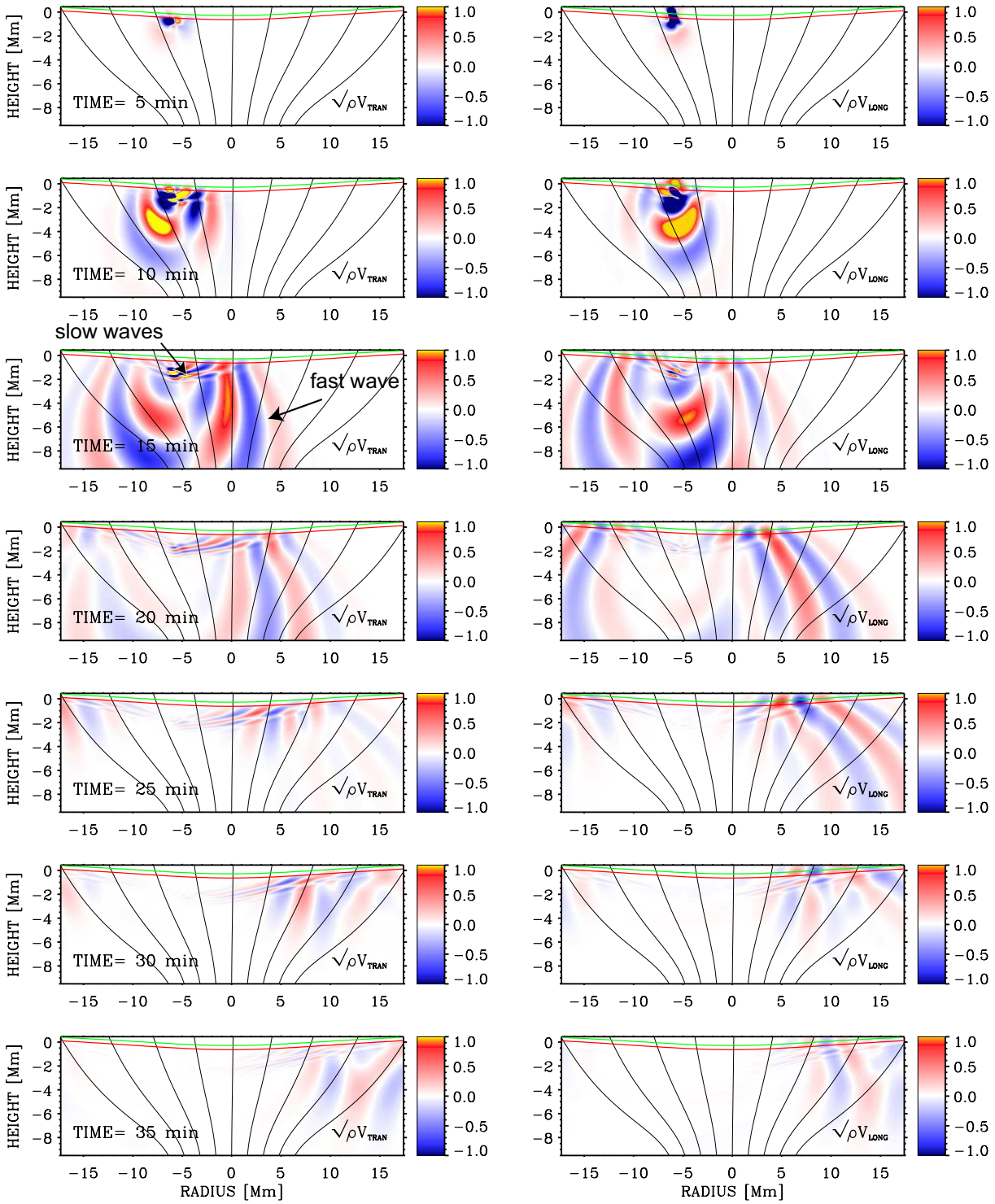

FIG. 5.— Time series of snapshots of the transversal (left panels) and longitudinal (right panels) velocities in the simulations with $B_{\rm phot}$ =1.5 kG and X_0 = 6 Mm. The velocities are scaled with the factor of $\sqrt{\rho_0}$. The color scales are the same in all panels. The red and green lines are contours of constant c_S^2/v_A^2, the red line corresponds to $v_A = c_S$, and the green line corresponds to $c_S^2/v_A^2 = 0.1$. The black inclined lines are the magnetic field lines. The negative heights correspond to sub-photospheric layers. Note the presence of slow waves, in addition to the modified p-modes (fast waves), indicated by arrows in the time = 15 min panel.

Gabor's wavelet:

$$G(\tau) = A\cos[\omega_0(\tau-\tau_p)]\exp\left[-\frac{\delta\omega^2}{4}(\tau-\tau_g)^2\right], \quad (8)$$

where A is the amplitude, ω_0 is the central frequency, τ_p and τ_g are the phase and group travel times respectively, and $\delta\omega$ is the bandwidth (Kosovichev & Duvall 1997). The fit has four free parameters: ω_0, τ_p, τ_g, and $\delta\omega$. The red curves plotted in the diagrams of Fig. 8 are the phase travel times τ_p obtained after the fit.

Fig. 9 shows the differences in the phase travel-times

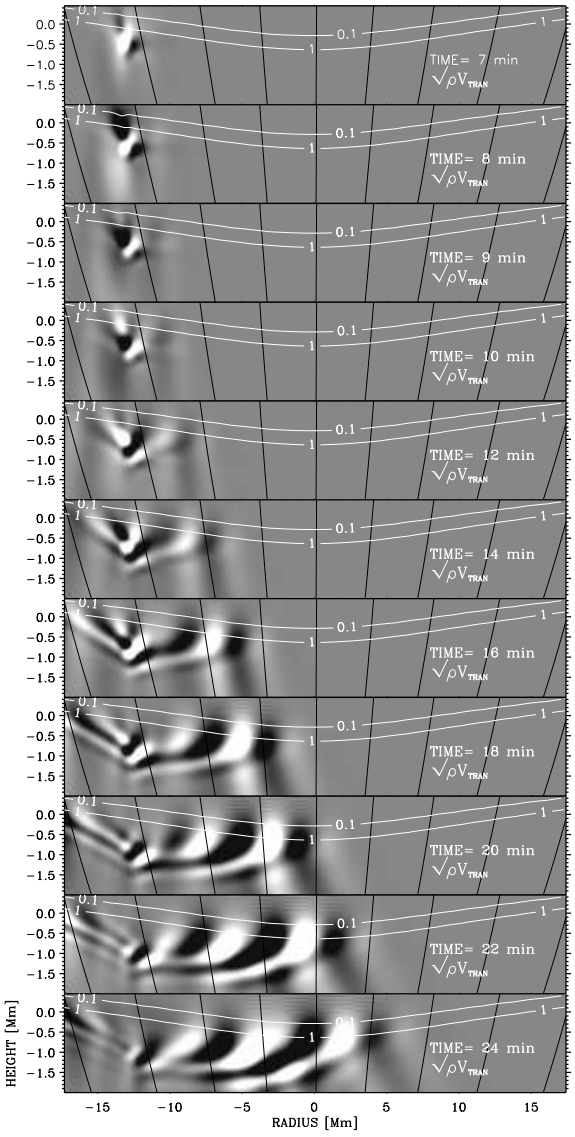

FIG. 6.— Time series of snapshots of the transversal velocity in the simulations with $B_{\rm phot}$ =1.5 kG and $X_0 = 12$ Mm. Only the top part of the simulation box is shown and the vertical axis has been expanded for better presentation. The velocities are scaled with the factor of $\sqrt{\rho_0}$. Each panel is normalized to its own maximum.

between the magnetic and non-magnetic simulations. Negative values mean that waves in the magnetic simulations propagate faster. The travel-time difference curves have a complex dependence on the distance. The difference between the magnetic and non-magnetic cases is larger at locations closer to the sunspot axis, where the magnetic field is stronger, and getting smaller at 15 Mm far from the axis. This happens because the waves with larger skip distances travel deeper inside the sunspot and are less affected by the magnetic surface effects. The travel time difference depends on the magnetic field strength of the model. The model with the smallest field $B_{\rm phot} = 0.9$ kG gives a maximum difference in the travel times of about 25 seconds, while in the model with the largest field strength $B_{\rm phot} = 2.4$ kG, this difference becomes about 35 seconds. The results presented in Figs. 8 and 9 are calculated for the photospheric vertical velocities taken at constant $\log\tau_5$ level. These results do not change much if we take velocities at a constant geometrical height $Z = 100$ km, instead of constant $\log\tau_5 = -1.6$. Only a minor additional phase shift is introduced in the travel time variations in Fig. 9 making them about 5 seconds smaller close to the sunspot axis.

The travel-time differences discussed above were calculated for the central frequency of the wave packet. However, there has been a discussion in the recent literature regarding the frequency dependence of the travel time measurements (Couvidat et al. 2006; Couvidat & Rajaguru 2007; Rajaguru 2008; Braun & Birch 2008). It has been obtained that, if the frequency filtering is applied to the data, in addition to the phase speed filtering, the resulting travel-time differences show a strong frequency dependence. High frequency waves have, in general, larger travel-time differences (Rajaguru 2008). In order to investigate this effect in our simulations, we filtered the simulated photospheric vertical velocities in the five frequency ranges: 3.3, 3.5, 4.0, 4.5 and 4.8 mHz. We applied a Gaussian filter with a FWHM of 1 mHz. The resulting travel-time differences are shown in Fig. 10, for all three model sunspots.

We find that the travel-time differences for each individual frequency behave similarly to the travel-time differences calculated without filtering. The maximum difference is achieved for distances closer to the sunspot axis (± 5 Mm), decreasing for the waves with large skip distances. A strong frequency dependence is evident from Fig. 10. Waves with higher frequencies have larger travel-time differences. It means that the propagation speed of waves increases with frequency. The magnitude of the frequency dependence that we obtain from the simulations is in agreement with the observations of Rajaguru (2008). In that paper travel-time differences change from, about, -15 to -30 seconds between 3 and 5 mHz, similar to our results in Fig. 10.

Interestingly, the travel-time differences get slightly positive for the distances within first $5 - 6$ Mm from the source location and for lower frequencies between 3.3 and 4.0 mHz. This effect needs further investigation.

5. EIKONAL APPROXIMATION SOLUTIONS

In order to understand more deeply the numerical results, we present here an approximate solution of the governing MHD equations for small perturbations in the eikonal approximation (see recent applications in *e.g.* McLaughlin & Hood 2006; McLaughlin et al. 2008; Khomenko & Collados 2006). The eikonal approach assumes that the wavelength of the perturbation is much smaller than the characteristic scale of the variations of the background model (Gough 2007). In the zero-order eikonal approximation, we neglect the variation of the wave amplitude and consider only the variation of its phase, i.e., we assume that all the variables in (1–4) depend on x, z and time as $U = a \cdot e^{i\phi(x,z)} \cdot e^{-i\omega t}$ (where a is constant). We make use of the recent developments of Cally (2006) and Moradi & Cally (2008) that allow to incorporate the effects of the acoustic cut-off frequency in the eikonal solution for MHD waves. In this approximation after some mathematical simplifications, the fol-

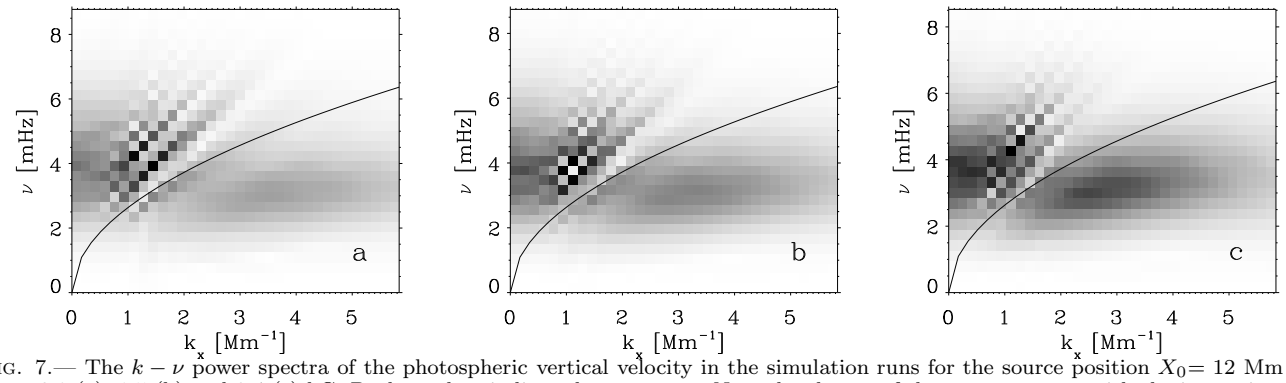

FIG. 7.— The $k-\nu$ power spectra of the photospheric vertical velocity in the simulation runs for the source position X_0= 12 Mm and $B_{\rm phot}$=0.9 (a), 1.5 (b) and 2.4 (c) kG. Darker colors indicate larger power. Note the change of the power spectra with the increasing field strength.

lowing first-order non-linear partial differential equation is obtained:

$$\begin{aligned} F(x,z,\phi,p,q) = & \omega^4 - \omega^2(c_S^2+v_A^2)(p^2+q^2) \\ & + c_S^2(p^2+q^2)(v_{Ax}p + v_{Az}q)^2 \\ & - \omega_c^2(\omega^2 - c_S^2 q^2) + c_S^2 N^2 p^2 = 0\,, \end{aligned} \tag{9}$$

where $p=\frac{\partial\phi}{\partial x}$ and $q=\frac{\partial\phi}{\partial z}$. Parameters p and q are equivalent to the horizontal and vertical wave numbers, respectively. Parameter N is the Brunt-Väisälä frequency, $N^2 = g/H - g^2/c_S^2$. In the following calculations, we use an expression for the cut-off frequency for an isothermal atmosphere $\omega_c = c_S/2H$. Equation (10) is solved by Charpit's method of characteristics by transforming it into the following system of ordinary differential equations:

$$\frac{dp}{ds} = -\frac{\partial F}{\partial x} \tag{10}$$

$$\frac{dq}{ds} = -\frac{\partial F}{\partial z} \tag{11}$$

$$\frac{dx}{ds} = \frac{\partial F}{\partial p} \tag{12}$$

$$\frac{dz}{ds} = \frac{\partial F}{\partial q} \tag{13}$$

Here, variable s is the distance along the characteristic wave propagation path. These four ODEs are solved numerically using a fourth-order Runge-Kutta method. We investigate only fast-mode solutions of the equations. Parameters c_S, v_A, N and ω_c are taken from the sunspot models. The solution of Eqs.(10–13) gives us $x(s)$, $z(s)$, $p(s)$ and $q(s)$ along the wave path s. The lines $x(z)$ give the trajectory of the group velocity of the solution. The phase along the wave path can be calculated as (Moradi & Cally 2008):

$$S(\vec{r}) = \int \vec{k} d\vec{r} - \omega t \tag{14}$$

where $\vec{r}=(x,z)$ and $\vec{k}=(p,q)$. The phase function $S(\vec{r})$ divided by the wave frequency ω gives us an estimate of the phase travel time.

First, we study the paths through the sunspot models of fast magneto-acoustic waves of a given frequency ω. Waves are launched from the same lower turning point at some depth below the surface. Fig. 11 gives the examples of solutions $x(z)$ for the fast wave paths for the frequencies 6.6 (top), 4.5 (middle) and 3.0 (bottom) mHz. As initial condition for the solution of the equations (10–13) we take in all the cases $x=-40$ Mm, $z=-3.5$ Mm and $q=0$. The initial value of p is found from the approximated solution of the dispersion relation (10) at $q=0$.

At each frequency, we calculate the wave paths for two cases. In the first case (red lines in Fig. 11) we set the Alfvén speed v_A to zero (*i.e.* eliminate the magnetic field), but keep the sound speed structure and frequencies N and ω_c from the sunspot model. In the second case, we calculate the wave path in the sunspot model taking into account magnetic field terms (white lines in Fig. 11). As can be observed in Fig. 11, the paths of the waves in the magnetic and non-magnetic cases are significantly different. Black dots on the curves mark the positions separated 1 minute in time in order to outline the quantitative differences in phase times spent by the waves on their paths.

The frequency of the wave at the top panel of Fig. 11 (6.6 mHz) is larger than the atmospheric cut-off. Thus, in the non-magnetic case, this wave (red line) propagates to the upper atmospheric layers without reflection and goes outside the simulation domain. This does not happen in the magnetic case. The green horizontal line in Fig. 11 marks the position of the layer where $c_S = v_A$. As the fast magneto-acoustic wave reaches this layer from below, its propagation properties become progressively more affected by the magnetic field. The fast magneto-acoustic wave in the region $v_A > c_S$ experiences the refraction due to the rapid increase of the v_A with height (a clear example of such behavior can be seen in the simulations presented by Khomenko & Collados 2006). Finally the fast magneto-acoustic wave reflects back to the deep layers at some height above the $c_S = v_A$. In the deep layers, this wave experiences again the refraction and reflection, but now due to the rapid increase of sound speed c_S. Thus, in this model, the high-frequency fast waves in the magnetic case are trapped below the photosphere due to magnetic effects.

If we reduce the wave frequency to 4.5 mHz (middle panel in Fig. 11), then in both the magnetic and non-magnetic cases the wave paths have an upper reflection point. The height where the wave frequency is equal to

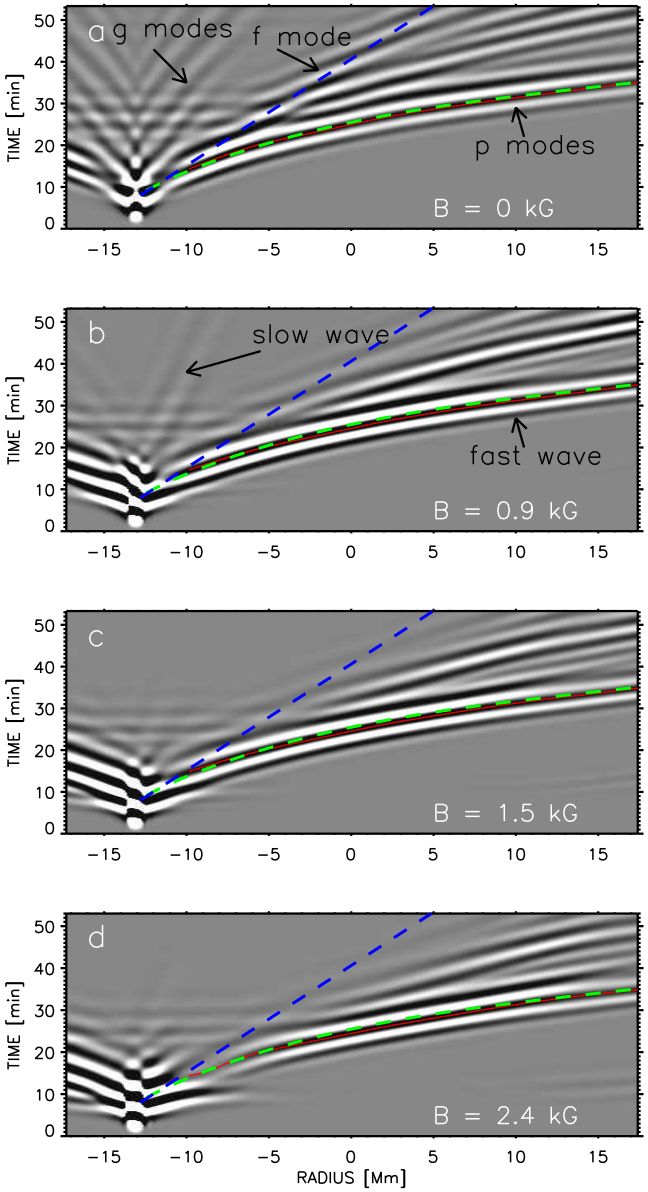

FIG. 8.— The time-distance diagrams of the photospheric vertical velocity for the simulations with (a) no magnetic field; (b) sunspot model with $B_{\rm phot} = 0.9$ kG; (c) sunspot model with $B_{\rm phot} = 1.5$ kG; (d) sunspot model with $B_{\rm phot} = 2.4$ kG. The source is located at $X_0 = 12$ Mm on the left of the sunspot axis. The red curves are the phase travel times calculated using the Gabor wavelet fit to the time-distance curves (see the text). The green dashed curves are theoretical time-distance curves for p-modes and the standard solar model S in the absence of the magnetic field. The blue dashed lines are the theoretical time-distance curves for the f mode calculated as $X = (1/2)(g/\omega)t$ for the central frequency $\omega = 2\pi/300$ of the wave source.

the atmospheric cut-off frequency is marked by the yellow lines in the figure. Since the sunspot model atmosphere has a temperature minimum, there is a region in between the two yellow lines, where the wave of frequency 4.5 mHz is evanescent. In the non-magnetic case, the wave is reflected sharply from this region. In the magnetic case, the reflection process is more complex. One can observe that the relative positions of the layer where $c_S = v_A$ and the cut-off (ω_c) layer change with the horizontal distance.

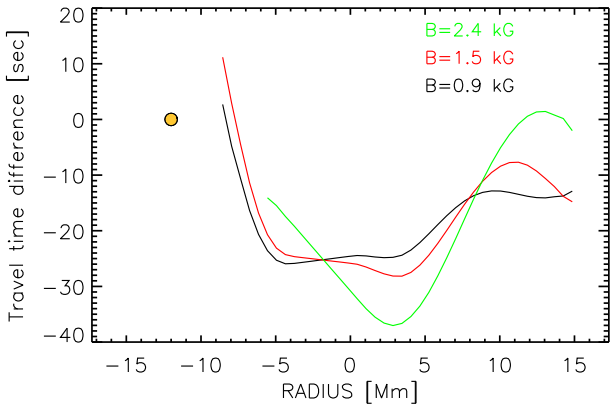

FIG. 9.— The phase travel-time difference calculated between the travel times measured in simulations without magnetic field and the simulations with different model sunspots (indicated in the figure) as a function of horizontal distance. The source location at $X_0 = 12$ Mm left to the sunspot axis is marked by yellow circle.

Far from the sunspot axis, where the field is relatively weak, the cut-off height lies below the $c_S = v_A$ layer. Thus, the waves are reflected before magnetic effects on the wave path take place. Note that the trajectories of the waves in the magnetic and non-magnetic cases are very similar in this region. As the waves approximate the region close to the sunspot center (where the magnetic field is large), the position of the $c_S = v_A$ layer lowers and the fast wave path becomes affected by the magnetic field. It can be seen from the figure that the red and white curves start to separate significantly in the region close to the sunspot axis. The waves in the magnetic case propagate with larger speeds and overtake the waves in the non-magnetic case. Note that by introducing the magnetic field, we have changed the height of the upper turning point of the waves. This may explain the shift of the positions of the ridges in the magnetic simulations in Fig. 7 compared to the non-magnetic simulations in Fig. 4.

Finally, the bottom panel of Fig. 11 gives the propagation paths in the low-frequency case of 3 mHz. In this case, the position of the cut-off height always lies below the height of $c_S = v_A$ layer. It means that (at least in our sunspot model atmosphere) low frequency waves are reflected before their path is significantly affected by the rapid increase of the Alfvén speed. However, it is important to note that even in this case, the trajectories of the waves in the magnetic and non-magnetic models are different. The propagation speed of the fast magneto-acoustic wave depends on the magnetic field and always greater than the sound speed.

6. QUANTITATIVE ESTIMATES OF THE TRAVEL TIMES AND SKIP DISTANCES

In order to quantify the effects of the magnetic field on the wave travel times in the eikonal approximation, we calculated the differences in travel times for the waves in the magnetic and non-magnetic cases. This calculation is done for waves frequencies between 3.3 and 4.8 mHz. The resulting travel time differences are presented in Fig. 12 as a function of the wave skip distance. This calculation is similar to the one reported by Moradi & Cally (2008).

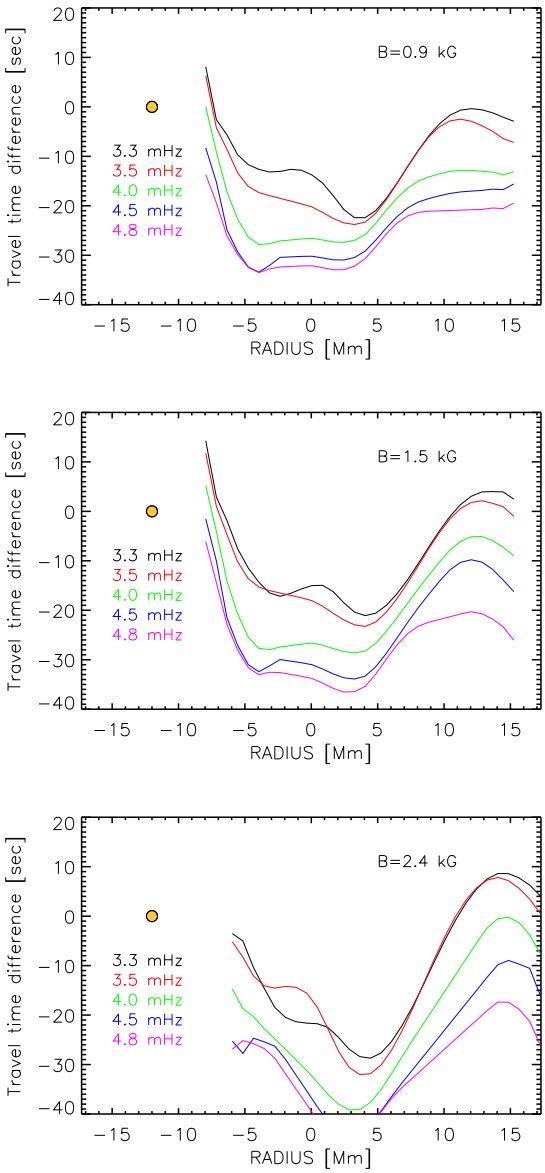

FIG. 10.— The phase travel time difference between the magnetic and non-magnetic cases as a function of the horizontal distance, calculated for different frequency filtering of the simulations with the source located at 12 Mm. The different colors correspond to different wave frequencies. Calculations done for the model sunspot with $B_{\rm phot} = 0.9$ kG (top), 1.5 kG (middle) and 2.4 kG (top).

The curves shown in Fig. 12 were calculated in the following way. In each case, the waves are launched from their lower turning point, thus $q = 0$, and p is obtained from the dispersion relation (10). The lower turning point is located at annuli distance $x_{\rm A} = 12$ Mm from the sunspot axis, in order to make the eikonal calculations directly comparable to the travel time estimates from simulations, as presented in Fig. 10. The vertical location of the lower turning point $z_{\rm A}$ varies in a range from -1.5 to -10 Mm below the photosphere. By varying $z_{\rm A}$ and frequency ω, we obtain different curves in Fig. 12. The deeper is $z_{\rm A}$, the larger is the value of the skip distance in the horizontal axis of Fig. 12. Note that to facilitate the comparison between the numerical simulations and the eikonal approach, we present the skip distances in Fig. 12 with respect to the position to the sunspot axis.

The frequency behavior calculated in the eikonal approximation is in good agreement with the simulations. It proves the reliability of the eikonal approximation for the full MHD approach. As in Fig. 10, the travel time differences are negative except for positions close to the source location, meaning that the waves propagate faster in the magnetic case. There is a strong frequency dependence of the travel time differences. Fig. 12 shows that depending on the sunspot model and on the skip distance, the maximum values change from, about, -50 sec for the 4.8 mHz wave to -10 sec for the 3.3 mHz wave. The agreement between simulations and the eikonal solution is worse in the $B_{\rm phot} = 2.4$ kG case, where the latter gives slightly larger values of the travel time differences and a different dependence. In all the cases the radius dependence obtained from the simulations using the Gabor wavelet fit is more complicated than the skip-distance dependence obtained in the eikonal approximation. Note that both simulations and the eikonal approximation give values of the travel time variations that fit reasonably well into the range of the observed values in solar active regions below sunspots (see, *e.g.* Kosovichev et al. 2000; Zhao & Kosovichev 2003; Couvidat et al. 2006; Couvidat & Rajaguru 2007; Braun & Birch 2008). However, the frequency dependence in the eikonal approximation is slightly larger than that obtained from simulations and observations.

7. DISCUSSION AND CONCLUSIONS

In this paper, we present an investigation of the influence of magnetic field on helioseismic wave propagation in active regions below sunspots. In order to better understand the physics of the waves in complex magnetic field configurations, we perform a single source experiment and study the propagation properties of the different wave modes excited by such a source, as well as the wave travel times. We have carried out our calculations in a series of sunspot models with different field strength and for two source positions located in magnetically and acoustically dominated regions. The results of our 2D simulations are compared to an asymptotic solution using the eikonal approximation. The results of both methods, numerical simulations and eikonal approximation, are found to be in a good qualitative agreement. Our approach has allowed us to investigate the effects of the magnetic field strength in sunspots on the travel-time variations obtained there from observations using the time-distance helioseismology techniques. In addition, the frequency dependence of such measurements has been studied.

The following conclusions summarize our study:

- The wave source located immediately below the surface in a non-magnetic standard solar model excites a mixture of p, f and g mode waves. When the magnetic field is present, the same source excites a mixture of fast and slow MHD waves. The fast modes represent an analog of the acoustic p modes, modified by the magnetic field.

- In addition to slow MHD waves excited directly by the source, there is another wave type with low

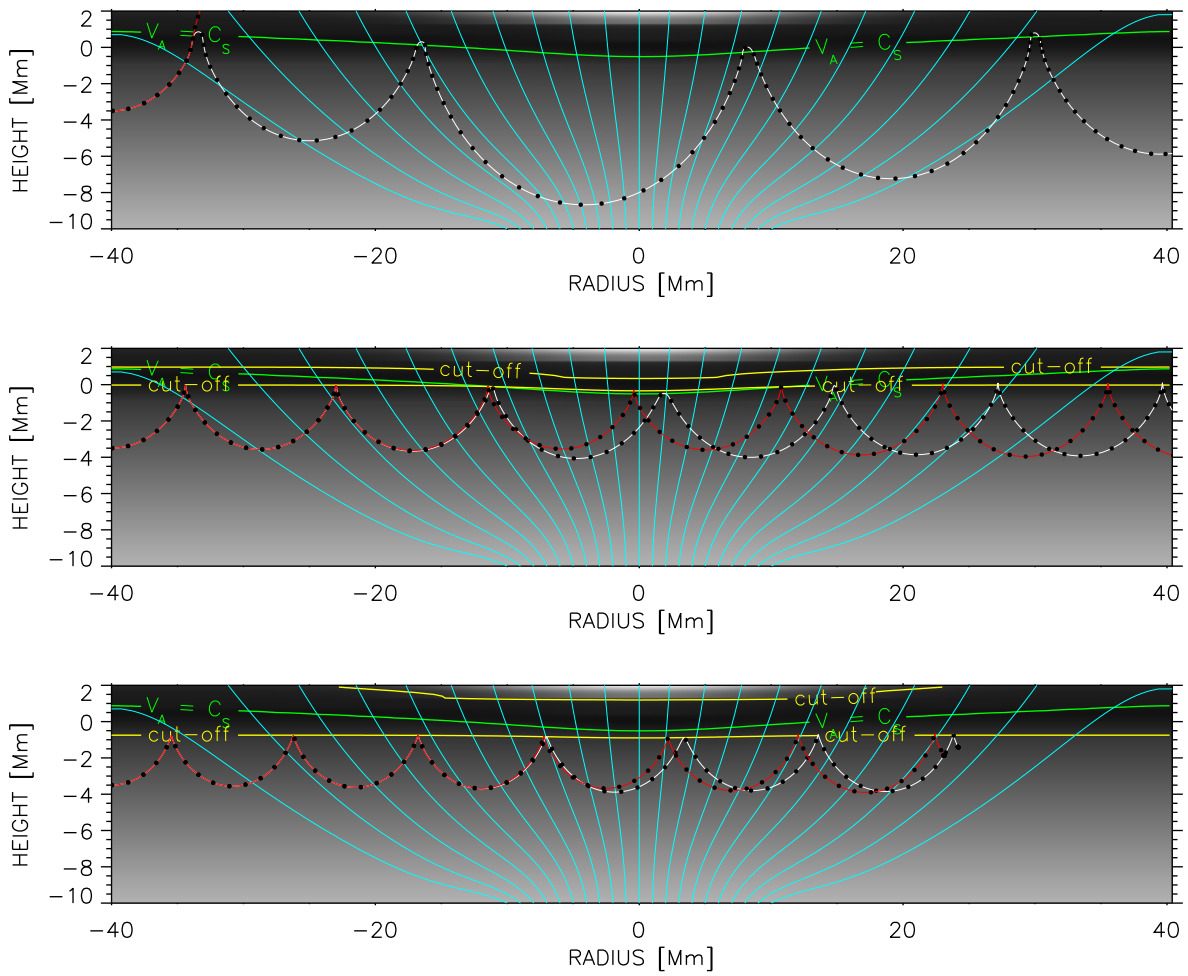

FIG. 11.— The wave paths of the fast mode waves launched from the same lower turning point below the photosphere propagating through the model sunspot with $B_{\rm phot} = 2.4$ kG for different frequencies: 6.6 mHz (top); 4.5 mHz (middle) and 3 mHz (bottom). The white curves are the wave paths when the magnetic field is taken into account. The red curves are the wave paths in the sunspot models with the same thermal properties, but setting $B = 0$. The black dots on the trajectory are separated from each other by 1 minute in time. The green curve marks the position of the $v_A = c_S$ layer. The yellow curves mark the heights where the frequency of the wave is equal to the local acoustic cut-off frequency. The background grey image is acoustic speed c_S.

vertical wavelength, propagating with speed close to that of the fast waves horizontally across the sunspot. We call them surface magneto-gravity waves. Several arguments listed in Sect. 4 indicate that these waves are different from either fast or slow waves. In our simulations these waves propagate below the visible surface. This makes their detection complicated in spectral observations.

- Slow MHD wave modes form an additional group of ridges in the time-distance diagram with much lower propagation speed. Their properties depend on the magnetic field strength of the model, as well as on the height in the atmosphere where the velocity is measured. The slow mode ridges on the time-distance diagrams are well isolated and do not affect the travel time measurements in magnetic regions.

- The helioseismic waves below sunspots are speed up by the magnetic field. The travel times of these waves are shorter by, about 20–40 seconds compared to the waves in the quiet Sun. Changing the photospheric magnetic field strength from 0.9 to 2.4 kG produces a variation of the travel times by about 10–15 seconds.

- Magnetic field produces a strong frequency dependence of the wave travel times. High frequency waves travel faster than low frequency waves. This happens because the propagation path of high frequency fast waves is modified strongly by the rapid increase of the Alfvén speed in the top layers, since these waves penetrate higher up in the atmosphere. Low frequency waves are reflected below the photosphere due to the acoustic cut-off frequency and do not reach the heights where $v_A > c_S$ and the magnetic fields produces strong effects. The travel time differences change from −20 to −35 seconds between 3 and 5 mHz, in agreement with observations (*e.g.* Rajaguru 2008).

The analysis presented here is limited by the 2D approximation. As a next step in our work we plan to relax

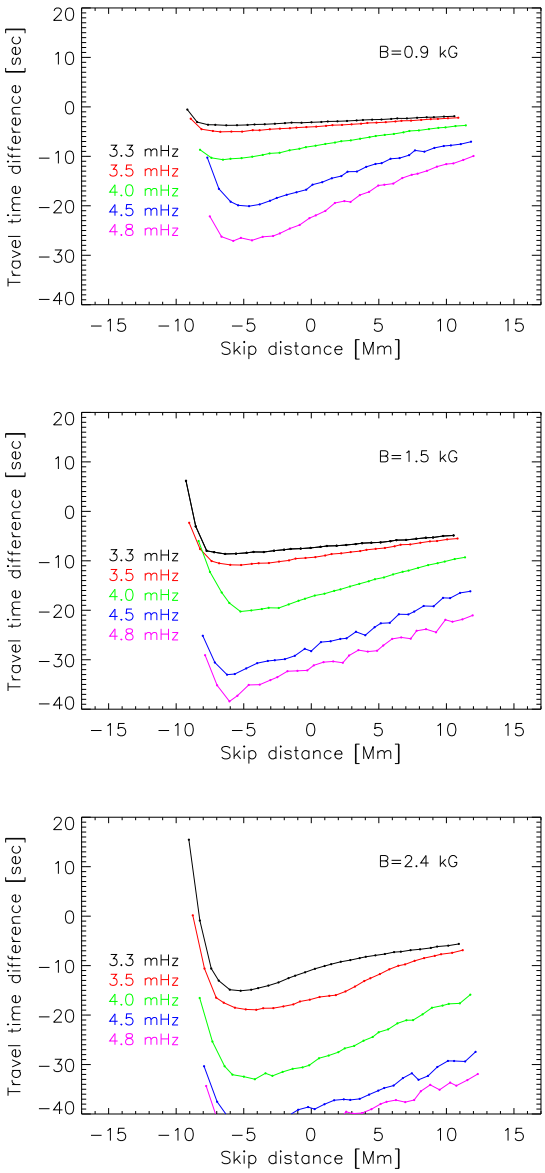

FIG. 12.— The travel time difference between magnetic and non-magnetic cases as a function of the skip distance, calculated in the eikonal approximation for the annuli size of 12 Mm. The lines of different colors correspond to different wave frequencies. The calculations are done for the sunspot models with $B_{\rm phot} = 0.9$ kG (top), 1.5 kG (middle) and 2.4 kG (top).

this assumption and to analyze 3D simulations, with a wave excitation by either single or multiple sources. This will allow us to build a more realistic picture and to complete our understanding of the interaction of helioseismic waves with magnetic fields of sunspots.

This research has been funded by the Spanish Ministerio de Educación y Ciencia through projects AYA2007-63881 and AYA2007-66502.

REFERENCES

Berenger, J. P. 1994, J. Comp. Phys., 114, 185
Birch, A. C. & Kosovichev, A. G. 2000, Solar Phys., 192, 193
Braun, D. C. 1997, ApJ, 487, 447
Braun, D. C. & Birch, A. C. 2008, Solar Phys., 251, 267
Braun, D. C. & Lindsey, C. 2000, Solar Phys., 192, 285
Cally, P. 2005, MNRAS, 358, 353
—. 2006, Phil. Trans. R. Soc. A, 364, 333
Cally, P. S. & Goossens, M. 2008, Solar Phys., 251, 251
Cameron, R., Gizon, L., & Daiffallah, K. 2007, Astron. Nach., 328, 313
Christensen-Dalsgaard, J., Dappen, W., Ajukov, S. V., & 30 co-authors. 1996, Science, 272, 1286
Couvidat, S., Birch, A. C., & Kosovichev, A. G. 2006, ApJ, 640, 516
Couvidat, S. & Rajaguru, S. 2007, ApJ, 661, 558
Crouch, A. D. & Cally, P. S. 2003, Solar Phys., 214, 201
Duvall, T. L. J., Jefferies, S. M., Harvey, J. W., & Pomerantz, M. A. 1993, Nature, 362, 430
Gizon, L. & Birch, A. C. 2002, ApJ, 571, 966
Gizon, L., Hanasoge, S. M., & Birch, A. C. 2006, ApJ, 643, 549
Gough, D. 2007, Astron. Nachr., 328, 273
Haber, D. A., Hindman, B. W., Toomre, J., Bogart, R. S., Thompson, M. J., & Hill, F. 2000, Solar Phys., 192, 335
Hanasoge, S. M. 2008, ApJ, 680, 1457
Hill, F. 1988, ApJ, 333, 996
Hindman, B. W., Jain, R., & Zweibel, E. G. 1997, ApJ, 476, 392
Jacoutot, L., Kosovichev, A. G., Wray, A., & Mansour, N. N. 2008, ApJ, 684, L51
Khomenko, E. & Collados, M. 2006, ApJ, 653, 739
—. 2008a, ApJ, in press
Khomenko, E., Collados, M, & Felipe, T. 2008, Solar Physics, 251, 589
Kosovichev, A. G. 1999, J. Comput. Appl. Math, 109, 1

—. 2002, Astron. Nachr., 323, 186
Kosovichev, A. G. & Duvall, T. L. J. 1997, in Solar Convection and Oscillations and their Relationship, ed. F. Pijpers, J. Christensen-Dalsgaard, & C. Rosenthal, Vol. 225, Astrophysics and Space Science Library (Kluwer Academic Publishers), 241—260
Kosovichev, A. G., Duvall, T. L. J., & Scherrer, P. H. 2000, Solar Phys., 192, 159
Lindsey, C. & Braun, D. C. 2005, ApJ, 620, 1107
Lindsey, C. & Braun, D. C. 2005, ApJ, 620, 1118
McLaughlin, J. A., Ferguson, J. S., & Hood, A. W. 2008, Solar Phys., 251, 563
McLaughlin, J. A. & Hood, A. W. 2006, A&A, 459, 641
Moradi, H. & Cally, P. 2008, Solar Phys., 251, 309
Parchevsky, K. V. & Kosovichev, A. G. 2007, ApJ, 666, 547
—. 2008, ApJ, submitted
Rajaguru, S. P., Sankarasubramanian, K., Wacher, R., & Scherrer, P. H. 2007, ApJ, 654, L175
Rajaguru, S. P. 2008, ApJ, submitted
Ruiz Cobo, B. & del Toro Iniesta, J. C., 1992, ApJ, 398, 375
Schunker, H., Braun, D. C., Cally, P. S., & Lindsey, C. 2005, ApJ, 621, L149
Schunker, H., Braun, D. C., Lindsey, C., & Cally, P. S. 2008, Solar Phys., 251, 341
Schunker, H. & Cally, P. S. 2006, MNRAS, 372, 551
Schwartz, R. A. & Stein, R. F. 1975, ApJ, 200, 499
Solanki, S. K. 2003, A&AR, 11, 153
Zhao, J. & Kosovichev, A. G. 2003, ApJ, 591, 446
—. 2006, ApJ, 643, 1317